International Symposium
On Turbulence and Shear Flow
Phenomena (TSFP-9)
June 30 - July 3, 2015 *Melbourne, Australia*

EVOLUTIONARY GEOMETRY OF LAGRANGIAN STRUCTURES IN THE TRANSITION OF THE COMPRESSIBLE BOUNDARY LAYER

Wenjie Zheng
State Key Laboratory of Turbulence and Complex Systems
College of Engineering, Peking University
Beijing 100871,China
jswj@pku.edu.cn

Yue Yang
State Key Laboratory of Turbulence and Complex Systems
College of Engineering, Peking University
Beijing 100871,China
yyg@pku.edu.cn

Shiyi Chen
State Key Laboratory of Turbulence and Complex Systems
College of Engineering, Peking University
Beijing 100871,China
syc@pku.edu.cn

ABSTRACT

We report a geometric study of evolving Lagrangian structures in a compressible transitional boundary layer at $Ma = 0.7$. The Lagrangian structures are extracted from the Lagrangian scalar field by a moving window filter. The multi-scale and multi-directional geometric analysis is applied to quantify and characterize the geometry of spatially evolving Lagrangian structures in the transition, including the averaged inclination and sweep angles at different scales ranging from one fifth of the boundary layer thickness δ to several viscous length scales δ_v. Here, the inclination angle is on the plane of the streamwise and wall-normal directions , and the sweep angle is on the plane of the streamwise and spanwise directions. The results show that, before the transition, averaged inclination and sweep angles are almost unaltered for different scales. As the transition occurs, averaged inclination angles increase and sweep angles decrease rapidly with increasing time for the structures with intermediate and small scales. In the late stage of transition, the averaged inclination angle of small-scale structures with the length scale $\sim O(10)\delta_v$ is $40^\circ - 50^\circ$, and the averaged sweep angle is approximately 30°.

INTRODUCTION

The flows near the wall have attracted extensive studies since Prandtl developed the boundary layer theory over 100 years ago. The spatially evolving, flat-plate transitional boundary layer flow, as a simple and typical wall flow, is widely studied with various applications ranging from engineering to meteorology.

Since the appearance of hairpin-shaped structures and hairpin packets is found in the transition of a number of boundary-layer flows (e.g., Wu & Moin (2009)), it is of importance to understand the underlying mechanism for the formation and evolution of the vortical structures, upon which predecessors have not reach a consensus (Marusic, 2009) and thus it is one of the principal future challenges (Wallace, 2013). The tracking of Lagrangian scalars, one of the Lagrangian-based approaches, may be helpful to elucidate the evolution of the hairpin-like structures. This method have been applied in isotropic turbulence (Yang et al., 2010), Taylor-Green and Kida-Pelz flows (Yang and Pullin, 2010), the K-type transition in channel flow (Zhao et al., 2015), and fully developed channel flows (Yang and Pullin, 2011). Note the flows in the previous Lagrangian studies mentioned are incompressible, and here we will extend this method to a compressible transitional wall flow.

In addition, the geometry of vortical structures in boundary layers is of interests for structure-based models of near-wall turbulence, but their accepted geometry is stil-l far from an agreement. With the tracking of Lagrangian scalar field, Yang & Pullin (2011) developed a multi-scale geometric analysis based on the mirror-extended curvelet transform (Candes, 2006). They present the temporal evolution of Lagrangian structures with quantitative multi-scale and multi-directional statistical geometry.

In the present study, we provide a Lagrangian perspective on a spatially evolving flat-plate boundary layer flow at $Ma = 0.7$. A moving window filter is proposed to extract the Lagrangian structures at different locations in the transition. Furthermore, the multi-scale and multi-directional geometric analysis is applied to characterize the evolutionary geometry of Lagrangian structures within the moving

window at different times and scales.

SIMULATION DETAILS

Direct Numerical Simulation

The direct numerical simulation (DNS) of a spatially evolving flat-plate boundary layer transition is performed by solving the three-dimensional compressible Navier-Stokes (N-S) equations with the OpenCFD code (Li et al., 2010). The N-S equations are integrated in time by using the third-order TVD type Runge-Kutta method. The convection terms are approximated by a seventh-order accuracy upwind finite difference scheme, and the viscous terms are approximated by an eighth-order accuracy central finite difference scheme. The flow parameters as well as mesh parameters are listed in Table 1, where the superscript '+' denotes a dimensionless quantity scaled by the viscous near-wall length scale $\delta_v = 0.0005$. Uniform meshes are used in the streamwise and spanwise directions, while exponentially stretched mesh is applied in the wall-normal direction to resolve the small-scale structures near the wall.

Table 1. DNS parameters

Ma	Re_∞	T_w
0.7	50000	1.098
$N_x \times N_y \times N_z$	$L_x \times L_y \times L_z$	$\Delta x^+ \times \Delta y_w^+ \times \Delta z^+$
$1000 \times 100 \times 320$	$10.00 \times 0.65 \times 1.57$	$19.98 \times 0.97 \times 9.80$

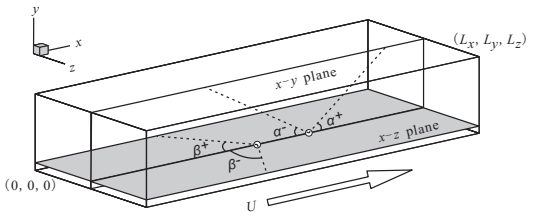

Figure 1. A schematic diagram of the computational domain and the characteristic angles of structures. Possible structures are sketched by dashed lines.

Figure 1 shows a diagram of the computational domain, where U is the mean velocity in the streamwise direction (x). The domain is bounded by inflow and outflow boundaries in the streamwise direction (x), a wall boundary and a (upper) non-reflecting boundary in the wall-normal direction (y), and two periodic boundaries in the spanwise direction (z). The details of these boundary conditions are listed as follows.

Inflow boundary. A laminar compressible boundary-layer similarity solution (White, 2006) with disturbances is imposed. Here, the disturbances are a two-dimensional Tollmien-Schlichting (T-S) wave and a couple of conjugate three-dimensional T-S waves to trigger the transition (Malik, 1990).

Outflow boundary. The non-reflecting boundary condition is imposed on all variables.

Wall boundary. The non-slip boundary condition is imposed together with the isothermal wall condition at the wall.

Figures 2 and 3 show the friction coefficient and the Reynolds number based on the friction velocity over the wall along the streamwise direction, perspectively. In the region $x = 4.5 - 8$ between laminar and turbulent regimes, there is a surge of the friction coefficient and the Reynolds number. This is hypothesized to be related to the appearance of three-dimensional vortices and the breakdown of large-scale coherent structures in the transition process. In addition, figure 4 shows the normalized mean Van Driest velocity profile at $x = 9.9$ with theoretical fittings.

Lagrangian Scalar Field

In the compressible flow, the three-dimensional Lagrangian scalar field $\phi(\boldsymbol{x},t)$ is governed by the passive scalar convection equation

$$\frac{\partial(\rho\phi)}{\partial t} + \nabla\cdot(\rho\boldsymbol{u}\phi) = 0. \tag{1}$$

After substituting the continuity equation into equation (1), we can obtain

$$\frac{\partial\phi}{\partial t} + \boldsymbol{u}\cdot\nabla\phi = 0, \tag{2}$$

which is the same as the one in incompressible flows (Yang et al., 2010; Yang and Pullin, 2011). Similarly, the trajectories of fluid particles can be calculated by solving the kinematic equation

$$\frac{\partial\boldsymbol{X}(\boldsymbol{x}_0,t_0|t)}{\partial t} = \boldsymbol{V}(\boldsymbol{x}_0,t_0|t) = \boldsymbol{u}(\boldsymbol{X}(\boldsymbol{x}_0,t_0|t),t), \tag{3}$$

where $\boldsymbol{X}(\boldsymbol{x}_0,t_0|t)$ is the location at time t of a fluid particle which was located at $\boldsymbol{x}_0$ at the initial time t_0. In equation (3), $\boldsymbol{V}(\boldsymbol{x}_0,t_0|t)$ is the Lagrangian velocity of the fluid particle, and $\boldsymbol{u}(\boldsymbol{X}(\boldsymbol{x}_0,t_0|t),t)$ is its local Eulerian velocity.

The backward-particle-tracking method (see Yang et al., 2010), which is stable and conserved, is used to calculate the Lagrangian scalar field as follows.
(1) The full Eulerian velocity field on the $N_x \times N_y \times N_z$ grid in a time interval from t_0 to $t(>t_0)$ is solved and stored.
(2) At a particular time t, particles are placed at the uniform grid points of $N_x^p \times N_y^p \times N_z^p$, and the initial Lagrangian field is given by $\phi_0 = y$. Here, the resolution of the Lagrangian field can be higher than that of the Eulerian velocity field in order to capture fine-scale Lagrangian structures.
(3) Particles are released and their trajectories are calculated backward in time until they arrive at $x = 1.0$. A three-dimensional, fourth-order Lagrangian interpolation scheme is used to obtain fluid velocity at the location of each particles, and an explicit, second-order Adams-Bashforth scheme is applied to carry out the time evolution.
(4) After the backward tracking, we can obtain initial locations of particles $\boldsymbol{x}_0$, which can be used to find the solution of $\phi(\boldsymbol{x},t)$ by a simple mapping

$$\phi(\boldsymbol{x},t) = \phi(\boldsymbol{X}(\boldsymbol{x}_0,t_0|t),t) \longleftrightarrow \phi_0. \tag{4}$$

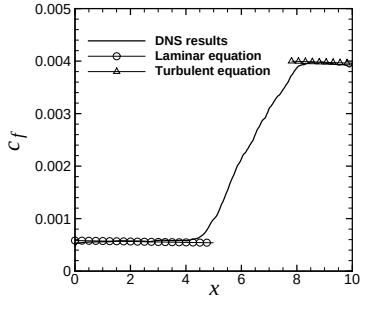

Figure 2. Skin-friction coefficient.

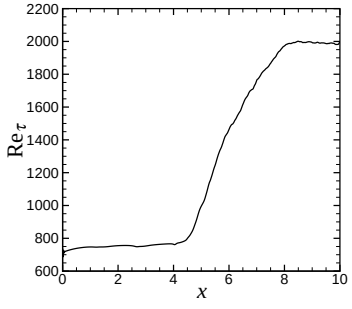

Figure 3. Friction Reynolds number.

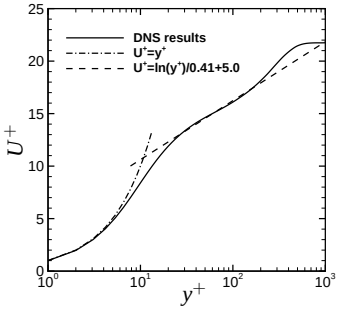

Figure 4. Mean Van Driest velocity profile normalized by the wall shear velocity at $x = 9.9$.

DIAGNOSTIC METHODOLOGIES

Multi-scale and Multi-directional Decomposition

A multi-scale and multi-directional filter based on the curvelet transform (Candes, 2006) is applied to a series of two-dimensional planes to quantify geometries of flow structures at multiple scales. Let the Fourier transform of an arbitrary two-dimensional scalar field $\varphi \in L^2(\mathbb{R}^2)$ be defined by

$$\hat{\varphi}(\boldsymbol{k}) = \frac{1}{2\pi}\int_{\mathbb{R}} \varphi(\boldsymbol{x}) \mathrm{e}^{-i\boldsymbol{k}\cdot\boldsymbol{x}} \mathrm{d}\boldsymbol{x}. \tag{5}$$

Then a filtered $\varphi(\boldsymbol{x})$ at scale j and along the direction l can be extracted from $\hat{\varphi}(\boldsymbol{k})$ in the Fourier space by the frequency window function

$$U_j(r,\theta) = 2^{-3j/4} W(2^{-j} r) V(t_l(\theta)) \tag{6}$$

with $r = \sqrt{k_1^2 + k_2^2}$ and $\theta = \arctan(k_2/k_1)$. Here $W(r)$ is the radial window function, and $V(t)$ is the angular window function. Numerical details can be referred to Yang & Pullin (2011).

The frequency windows cover the whole Fourier domain at characteristic length scales $\mathscr{L}_j = 2^{-j}, j \in \mathbb{N}_0$ and the equispaced sequence of rotation angles $\theta_{j,l} = \pi l 2^{-\lceil j/2 \rceil}/2, 0 \leqslant l \leqslant 4 \cdot 2^{\lceil j/2 \rceil} - 1$. Part of the normalized characteristic length scales of structures after filtering is given in Table 2.

Table 2. Characteristic length scales

Length	Scale 3	Scale 4	Scale 5	Scale 6
$\mathscr{L}_j/\delta$	0.192	0.096	0.048	0.024
$\mathscr{L}_j/\delta_v$	250	125	62.5	31.25

The multi-scale decomposition of the original scalar field $\varphi(\boldsymbol{x})$ can be obtained by applying the radial window function $W(r)$ on $\hat{\varphi}(\boldsymbol{k})$ as

$$\varphi_j(\boldsymbol{x}) = \int \hat{\varphi}(\boldsymbol{k}) W(2^{-j} r) \mathrm{e}^{i\boldsymbol{k}\cdot\boldsymbol{x}} \mathrm{d}\boldsymbol{k} \tag{7}$$

for each scale j.

For scale j, the orientation information of $\varphi(\boldsymbol{x})$ can be represented by the averaged deviation angles away from the horizontal axis in the physical space

$$\langle \Delta\theta \rangle_j^+ = \frac{\sum_{l'=0}^{l'_{max}} \Phi_j(\Delta\theta)\Delta\theta}{\sum_{l'=0}^{l'_{max}} \Phi_j(\Delta\theta)} \tag{8}$$

and

$$\langle \Delta\theta \rangle_j^- = \frac{\sum_{l'=l'_{min}}^{0} \Phi_j(\Delta\theta)\Delta\theta}{\sum_{l'=l'_{min}}^{0} \Phi_j(\Delta\theta)} \tag{9}$$

with $l'_{min} = -2^{\lceil j/2 \rceil}$ and $l'_{max} = 2^{\lceil j/2 \rceil}$. Here, $\Phi_j(\Delta\theta) = \frac{\int \hat{\varphi}(\boldsymbol{k}) U_j(r,\theta) \mathrm{d}\boldsymbol{k}}{\int U_j(r,\theta) \mathrm{d}\boldsymbol{k}}$ is the normalized angular spectrum, and $\Delta\theta = \pi l' 2^{-\lceil j/2 \rceil}/2, -2^{\lceil j/2 \rceil} \leqslant l' \leqslant 2^{\lceil j/2 \rceil}$ is the discrete deviation angle away from the horizontal axis.

When a scalar field has non-periodic boundaries, such as φ on the $x-y$ plane in the compressible boundary layer, the fast Fourier transform (FFT) may result in artificial oscillation near boundaries. In practice, we copy and flip the two-dimensional scalar field by the one-dimensional mirror extension in the wall-normal direction as

$$\{\varphi_1, \ldots, \varphi_N\} \to \{\varphi_1, \ldots, \varphi_N, \varphi_{N-1}, \ldots, \varphi_2\} \tag{10}$$

before the FFT, while the streamwise direction with non-periodic boundary conditions will be resolved in the next section.

Moving Window Filter

A moving window filter is applied to extract the evolving Lagrangian structure at different locations. Here, the filter is defined by an exponential function as

$$f(x,t) = \exp\left[-n\left(\frac{x - x_c(t)}{l_w(t)}\right)^n\right], \tag{11}$$

where x_c is the central position of the window, and l_w is the window length.

The filter with growing filter width travels along the streamwise direction at a certain speed in the compressible

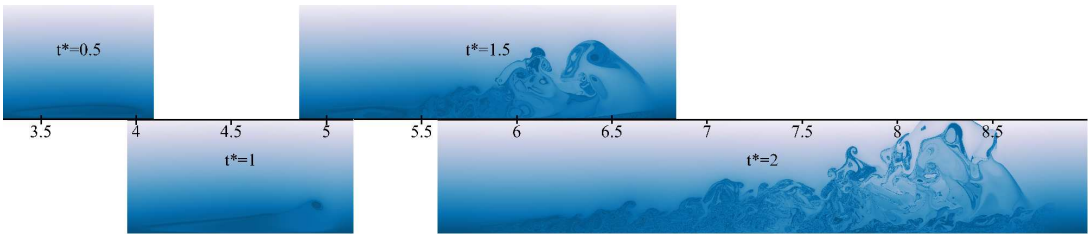

Figure 5. Evolution of Lagrangian structures on the $x-y$ plane ($z=0.785$) in a compressible transitional boundary layer ($Ma=0.7$).

transitional boundary layer. Since it can follow and capture the flow evolution, the Lagrangian field in the moving frame becomes statistically time-dependent (Pope, 2000). The scaled time $t^*=(t-t_0)/T$ is normalized by the period T of the T-S waves imposed at the inlet boundary. It is noted that $x_c(t^*)$ and $l_w(t^*)$ can be fitted by quadratic polynomials from the DNS results.

With given $x_c(t^*)$ and $l_w(t^*)$, the extracted Lagrangian scalar field $\phi_f(\boldsymbol{x})$ at time t^* can be obtained as

$$\phi_f(\boldsymbol{x})=\phi(\boldsymbol{x})f+\phi_0(\boldsymbol{x})(1-f). \tag{12}$$

Thus the extracted Lagrangian field is within the moving window with the smooth transition from the evolving scalar to the initial scalar at boundaries, so that the boundary condition in the streamwise direction in the frame can be considered as periodic for the FFT.

LAGRANGIAN STRUCTURES

Geometry of Lagrangian Structures on the Streamwise and Wall-normal Plane

By applying the moving window filter on the Lagrangian field $\phi(\boldsymbol{x},t)$ in the compressible boundary layer, a filtered Lagrangian field $\phi_f(\boldsymbol{x},t^*)$ can be extracted at a sequence of non-dimensional times t^*. Typical snapshots on the $x-y$ plane at different t^* are shown in figure 5.

The temporal evolution of the Lagrangian structures on the $x-y$ plane in the transitional compressible boundary layer is shown in figure 6. We can see that the initial large-scale, bulge-shaped structure in figure 6(a) is lifted and stretched to form a hairpin-shaped structure in the near wall region, as shown in figure 6(b). Under the mean flow shear stress, the hairpin-shaped structure in figure 6(c) is stretched and its head lifts away from the wall owing to its self-induction governed by the Biot-Sarvart law, which leads to the shear stress around the head keeps increasing. When the shear stress exceeds a threshold value, the large-scale hairpin-shaped structure breaks down at the neck region into a packet of small-scale structures in figure 6(d).

As shown in figure 1, we define the inclination angle α between an inclined structure projected on the $x-y$ plane and the x-direction. In terms of the variables in the multi-scale and multi-directional decomposition, we have $\phi_f(x,y,z=z_p)\leftrightarrow\varphi$, $\alpha^+\leftrightarrow\langle\Delta\theta\rangle^+$ and $\alpha^-\leftrightarrow\langle\Delta\theta\rangle^-$. Evolution of the Lagrangian field at each scale can be obtained using the scale decomposition of $\phi_f(\boldsymbol{x},t^*)$ on the $x-y$ plane by equation (7). For example, the evolution of the small-scale structure with $j=6$ is shown in figure 7, where the characteristic length scale for each scale index j is quantified in Table 2. Then, the orientation statistics of $\phi_f(\boldsymbol{x},t^*)$ on the $x-y$ plane at different scales can be obtained by the averaged deviation angles defined by equations (8) and (9).

We define the averaged inclination angle $\langle\alpha\rangle=(\langle\alpha^+\rangle+\langle\alpha^-\rangle)/2$. Figure 8 shows the temporal evolution of $\langle\alpha\rangle$ for Lagrangian structures at intermediate and small scales. As shown in figure 7(a), the small-scale structures with small $\langle\alpha\rangle$ appear at early times. Then, the small-scale structures are lifted in figures 7(b)-7(d). In figure 8, we can find that $\langle\alpha\rangle$ grows slowly with time, and the difference for different scales is smaller than 5° before $t^*=1$. After $t^*=1$, $\langle\alpha\rangle$ begins to increase significantly with increasing time, which corresponds to the occurrence of the transition. The increasing trend of the large-scale structures with the length scale 0.2δ is slower than those of small-scale structures with the length scale $\sim O(10)\delta_v$. Moreover, the averaged inclination angles grow from 15° to 50° nearly in the same rate for Lagrangian structures at scales smaller than $60\delta_v$. When the flow reaches the fully-developed turbulent region around $t^*=2$, the averaged inclination angle of small-scale structures with the length scale $\sim O(10)\delta_v$ is $40^\circ-50^\circ$.

Geometry of Lagrangian Structures on the Streamwise and Spanwise Plane

The temporal evolution of the Lagrangian field on the $x-z$ plane at $y^+=120$ in the compressible boundary layer is shown in figure 9. We can see that the initial large-scale triangle-shaped structure in figure 9(a) is stretched into a packet of small-scale Λ-shaped structures in figure 9(d).

As shown in figure 1, the sweep angle β is between the structure and the streamwise direction on the $x-z$ plane. In terms of the variables in the multi-scale and multi-directional decomposition, we have $\phi_f(x,y=y_p,z)\leftrightarrow\varphi$, $\beta^+\leftrightarrow\langle\Delta\theta\rangle^+$, and $\beta^-\leftrightarrow\langle\Delta\theta\rangle^-$.

Evolution of the typical small-scale Lagrangian structures at scale $j=6$ is shown in figures 10. We define the averaged sweep angle $\langle\beta\rangle=(\langle\beta^+\rangle+\langle\beta^-\rangle)/2$. The temporal evolution of $\langle\beta\rangle$ for Lagrangian structures at different scales is shown in figure 11. As shown in figure 10(a), the small-scale structures with large $\langle\beta\rangle$ appear at early times. Then, the small-scale structures are stretched along the streamwise in figures 10(b)-10(d). In figure 11, we can find that $\langle\beta\rangle\approx90^\circ$ at early times, which illustrates the Lagrangian field is essentially two-component in three-dimensional physical space. Before $t^*=1$, $\langle\beta\rangle$ decreases slowly with time for the structures at all the scales. Similar to the averaged inclination angle in figure 8, $\langle\beta\rangle$ decreases rapidly with increasing time after $t^*=1$, which corresponds to the beginning of the transition. It is noted that the decrease of $\langle\beta\rangle$ for the large-scale structures with the length scale 0.2δ is much smaller than those with the small length scale $\sim O(10)\delta_v$. The decreasing trend of $\langle\beta\rangle$ gradually s-

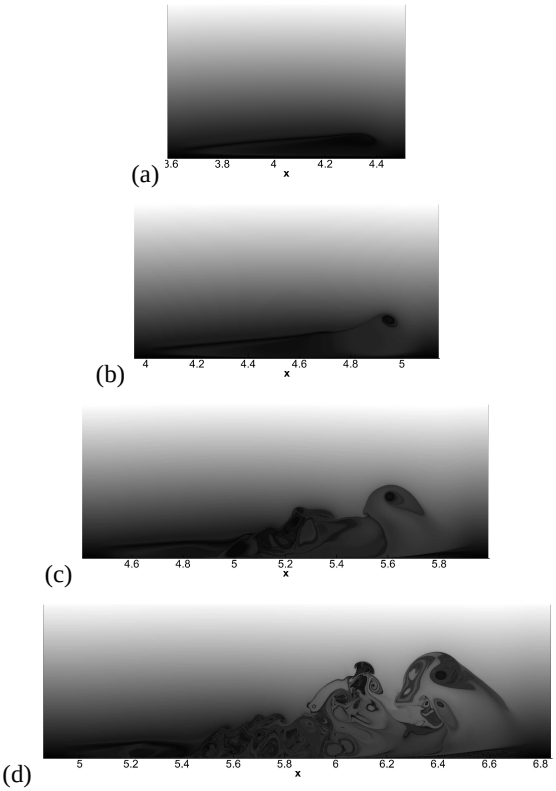

Figure 6. Evolution of Lagrangian structures on the $x-y$ plane ($0 \leqslant y \leqslant 0.6, z = 0.785$) in a compressible transitional boundary layer ($Ma = 0.7$). (a) $t^* = 0.75$, (b) $t^* = 1$, (c) $t^* = 1.25$, (d) $t^* = 1.5$.

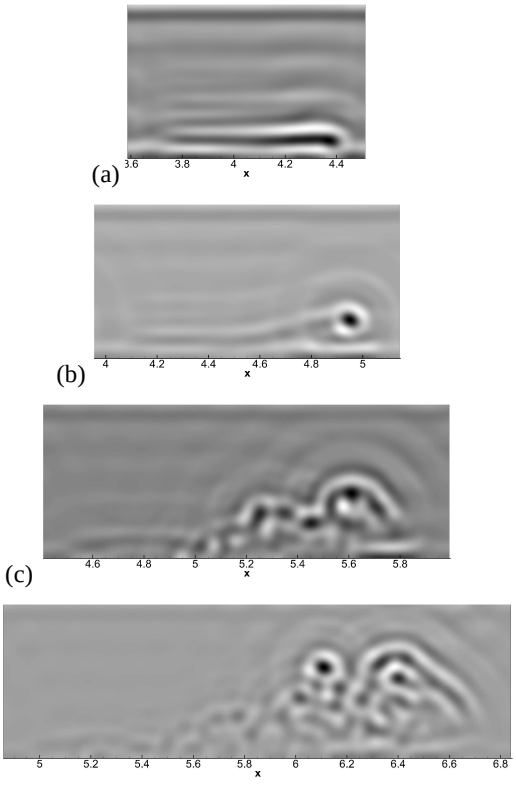

Figure 7. Evolution of Lagrangian structures at scale 6 on the $x-y$ plane ($0 \leqslant y \leqslant 0.6, z = 0.785$) in a compressible transitional boundary layer ($Ma = 0.7$). (a) $t^* = 0.75$, (b) $t^* = 1$, (c) $t^* = 1.25$, (d) $t^* = 1.5$.

lows down after $t^* \geq 1.5$. When $t^* = 2$, the sweep angle of the small-scale structures is approximately 30°.

CONCLUSIONS

The Lagrangian scalar field developed in incompressible flows is extended to a compressible transitional boundary layer flow. Based on the Lagrangian field, a moving window filter is developed to extract the spatially evolving Lagrangian structures at a time sequence. The multi-scale and multi-directional geometric analysis is then applied to characterize the evolutionary geometry of Lagrangian structures in the transition, including the averaged inclination and sweep angles at different scales. Before the transition, averaged inclination and sweep angles are almost unaltered for different scales. As the transition occurs, the averaged inclination angle increases and the averaged sweep angle decreases rapidly with increasing time for the structures with the length scale smaller than 0.1δ. In addition, the increasing or decreasing trend are very similar for Lagrangian structures at scales smaller than $60\delta_v$. In the late stage of transition, the averaged inclination angle of small-scale structures with the length scale $\sim O(10)\delta_v$ is $40^\circ - 50^\circ$, and the averaged sweep angle is approximately 30°. The effects of the Mach number on the evolution and geometry of Lagrangian structures will be investigated in the future.

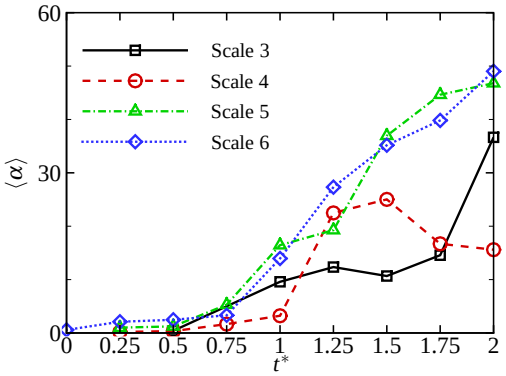

Figure 8. Evolution of the averaged inclination angle (degrees) in a compressible transitional boundary layer ($Ma = 0.7$).

REFERENCES

Candes, E., Demanet, L., Donoho, D. & Ying, L. 2006 Fast discrete curvelet transforms. *Multiscale Modeling and Simulation* **5**, 861–899.

Li, X. L., Fu, D. X. & Ma, Y. W. 2010 Direct numerical simulation of hypersonic boundary layer transition over a blunt cone with a small angle of attack. *Physics of Fluids* **22**, 025105.

Malik, M. R. 1990 Numerical methods for hypersonic boundary layer stability. *Journal of Computational*

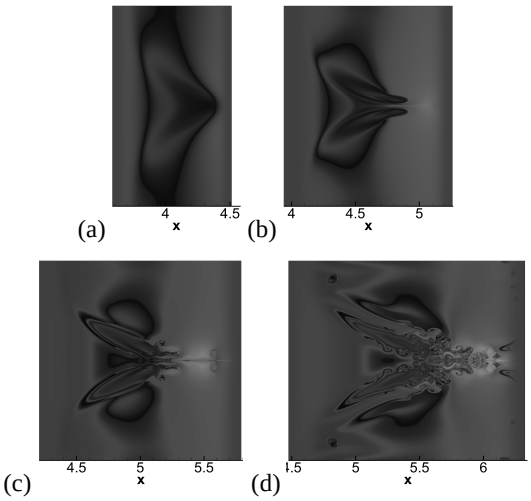

Figure 9. Evolution of Lagrangian structures on the $x-z$ plane ($0 \leqslant z \leqslant 1.57, y^+ = 120$) in a compressible transitional boundary layer ($Ma = 0.7$). (a) $t^* = 0.75$, (b) $t^* = 1$, (c) $t^* = 1.25$, (d) $t^* = 1.5$.

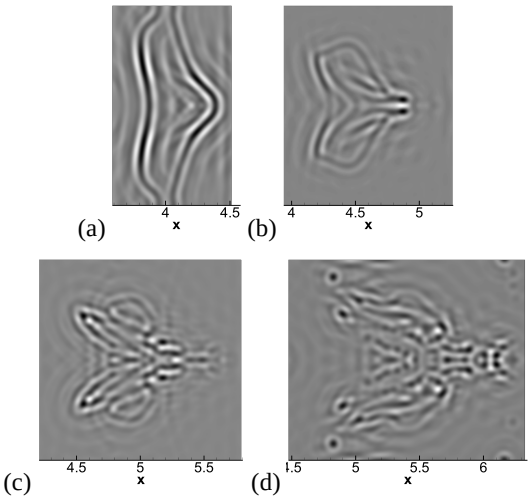

Figure 10. Evolution of Lagrangian structures at scale 6 on the $x-z$ plane ($0 \leqslant z \leqslant 1.57, y^+ = 120$) in a compressible transitional boundary layer ($Ma = 0.7$). (a) $t^* = 0.75$, (b) $t^* = 1$, (c) $t^* = 1.25$, (d) $t^* = 1.5$.

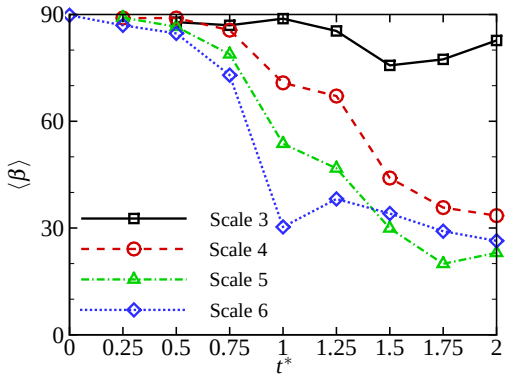

Figure 11. Evolution of the averaged sweep angle (degrees) in a compressible transitional boundary layer ($Ma = 0.7$).

Physics **86**, 376–413.

Marusic, I. 2009 Unravelling turbulence near walls. *Journal of Fluid Mechanics* **630**, 1–4.

Pope, S. B. 2000 *Turbulent Flows*. Cambridge University Press.

Wallace, J. M. 2013 Highlights from 50 years of turbulent boundary layer research. *Journal of Turbulence* **13**, 1–70.

White, F. M. 2006 *Viscous Fluid Flow*, 3rd edn. McGraw-Hill.

Wu, X. H. & Moin, P. 2009 Direct numerical simulation of turbulence in a nominally zero-pressure-gradient flat-plate boundary layer. *Journal of Fluid Mechanics* **630**, 5–41.

Yang, Y. & Pullin, D. I. 2010 On lagrangian and vortex-surface fields for flows with taylor-green and kida-pelz initial conditions. *Journal of Fluid Mechanics* **661**, 446–481.

Yang, Y. & Pullin, D. I. 2011 Geometric study of lagrangian and eulerian structures in turbulent channel flow. *Journal of Fluid Mechanics* **674**, 67–92.

Yang, Y., Pullin, D. I. & Bermejo-Moreno, I. 2010 Multi-scale geometric analysis of lagrangian structures in isotropic turbulence. *Journal of Fluid Mechanics* **654**, 233–270.

Zhao, Y., Yang, Y. & Chen, S. 2015 Evolution of lagrangian structures in the temporal transition in channel flow (under review) .